

# IRAC Observations of Taurus Pre-Main Sequence Stars

Lee Hartmann<sup>1</sup>, S.T. Megeath<sup>1</sup>, Lori Allen<sup>1</sup>, Kevin Luhman<sup>1</sup>, Nuria Calvet<sup>1</sup>, Paola D'Alessio<sup>2</sup>,  
Ramiro Franco-Hernandez<sup>2</sup>, Giovanni Fazio<sup>1</sup>

hartmann@cfa.harvard.edu

## ABSTRACT

We present infrared photometry obtained with the IRAC camera on the *Spitzer* Space Telescope of a sample of 82 pre-main sequence stars and brown dwarfs in the Taurus star-forming region. We find a clear separation in some IRAC color-color diagrams between objects with and without disks. A few “transition” objects are noted, which correspond to systems in which the inner disk has been evacuated of small dust. Separating pure disk systems from objects with remnant protostellar envelopes is more difficult at IRAC wavelengths, especially for objects with infall at low rates and large angular momenta. Our results generally confirm the IRAC color classification scheme used in previous papers by Allen et al. and Megeath et al. to distinguish between protostars, T Tauri stars with disks, and young stars without (inner) disks. The observed IRAC colors are in good agreement with recent improved disk models, and in general accord with models for protostellar envelopes derived from analyzing a larger wavelength region. We also comment on a few Taurus objects of special interest. Our results should be useful for interpreting IRAC results in other, less well-studied star-forming regions.

*Subject headings:* accretion disks - infrared: stars - stars: formation - stars: pre-main sequence

## 1. Introduction

The Taurus-Auriga molecular cloud has long served as a touchstone for understanding pre-main sequence evolution. The proximity of Taurus, plus the relatively low extinction in the area, has enabled researchers to develop a reasonably complete census of the pre-main sequence population. These properties also mean that the characterization of protostellar envelopes and circumstellar disks is more extensive and detailed for Taurus objects than for any other star-forming region (see, e.g., Kenyon & Hartmann 1995 = KH95).

---

<sup>1</sup>Center for Astrophysics, 60 Garden Street, Cambridge, MA 02138

<sup>2</sup>Centro de Radioastronomía y Astrofísica, Ap. P. 72-3 (Xangari) 58089 Morelia, Michoacan, Mexico

We are conducting a survey of known Taurus pre-main sequence stars using the IRAC camera on board the *Spitzer* Space Telescope. Although a great deal is already known about the infrared spectral energy distributions (SEDs) of Taurus members, the unprecedented photometric sensitivity of IRAC in the mid-infrared permits the study of many more objects in the  $\sim 3 - 9\mu\text{m}$  wavelength range than previously possible from ground-based studies. The IRAC data also provide an important link between measurements of stellar photospheric emission (which generally peaks at around  $1\mu\text{m}$ ) and forthcoming detailed spectra of Taurus members obtained with the IRS spectrograph on *Spitzer* (which covers the  $\sim 5 - 35\mu\text{m}$  range). More broadly, our IRAC observations of previously well-characterized systems in Taurus can serve as a guide to the interpretation of IRAC data of other, much more distant regions which can now be studied with the unparalleled sensitivity of *Spitzer*.

In this paper we report preliminary results from our IRAC survey, with results for 82 Taurus systems. A fuller accounting of the  $\sim 200$  pre-main sequence Taurus systems in the IRAC Guaranteed Time program will be published later, as data become available.

## 2. Observations

The observations reported here were obtained with the IRAC instrument on board the *Spitzer* Space Telescope (Fazio et al. 2004). IRAC observations are made with four filters; here we refer to them by their approximate wavelength centers of 3.6, 4.5, 5.8, and  $8\mu\text{m}$ . A sequence of observations in all four filter bands requires a minimum of two pointings for a given target, since each of the two IRAC fields of view serves two imaging channels. For all of the observations reported here, we made three spatial dithers in each band to improve signal-to-noise and cosmic ray rejection. We used the “High Dynamic Range” (HDR) 12 second integration mode, which involves taking two frames with effective exposure times of 10.4 and 0.4 seconds.

The pre-main sequence stars in Taurus are widely dispersed on the sky. This means that mapping methods are inefficient except in some regions such as L1551 and L1495 (which will be reported separately). The observations reported here were mostly taken in “cluster mode”, which involves identifying individual targets clustered within a one degree radius of a common center. In all but a few cases, only one Taurus member (system) was observed in a single IRAC field.

The Taurus data were taken during two IRAC “campaigns” on February 9-14, 2004, and March 6-9, 2004. For comparison we include IRAC data for the interesting 10 Myr-old star TW Hya, taken on Dec. 20, 2003.

The data frames were processed by the pipeline version S9.5 at the *Spitzer* Science Center. Photometry was extracted from the basic calibrated data frames using the aperture photometry routine `aper.pro` in the IDLPHOT package (Landsman 1993). The IDLPHOT routines were integrated into a custom IDL program which use the WCS information in the image headers to identify the images containing a given star and find the star within the images. The program then obtains

the centroid of the star and extracts the photometry. A 5 pixel aperture was used for each star, with a sky annulus extending from 5 pixels to 10 pixels. Since the zero points are referenced to a star measured with a 10 pixel aperture and a sky annulus spanning radii from 10 to 20 pixels, we scaled the photometry with an aperture correction derived from calibration star data. The corrections used were 1.061, 1.064, 1.067, and 1.089 in the [3.6], [4.5], [5.8], and [8] bands, respectively. Instrumental magnitudes were measured from each of the three dithered images independently. The quoted values are the mean of the three magnitudes, and the quoted standard deviations are the observed standard deviation in the three frames.

For binaries with separations on the order of  $2-12''$ , photometry was performed by fitting point spread functions to the two objects simultaneously using a custom IDL program. The point spread function (PSF) used were those derived from the Campaign Q data, given at the *Spitzer* Science Center website (<http://ssc.spitzer.caltech.edu/irac/psf.html>). For each binary system, PSF fitting was performed individually on all three dithered images taken. PSF fitting photometry was also obtained for a sample of ten, isolated stars, and the mean offset between the magnitudes returned by the PSF fitting and the aperture photometry routines was measured. The PSF fitting magnitudes were corrected by this offset to ensure consistency with the aperture photometry reported for all the isolated stars. The reported uncertainty of the PSF fitting photometry is the standard deviation of the magnitudes determined for each of the three dithers added in quadrature with the uncertainty in the offset between the aperture and PSF fitting photometry.

We adopted zero point magnitudes ( $ZP$ ) of 19.660, 18.944, 16.880, 17.394 in the [3.6], [4.5], [5.8] and [8] bands, respectively, where  $[m] = -2.5 \log(DN/sec) + ZP$ . These were derived from the average calibration of four AV star primary standards, HD165459, NPM1p64.0581, 2MASS1812095, and NPM1p60.0581, which are observed during every IRAC campaign. By adopting these zero points, the resulting IRAC colors of the A dwarfs were equal to 0, as expected in the Vega-based IRAC magnitude system. We estimate uncertainties in the zero point magnitudes of approximately 0.05 mag; repeatability appears to be at the level of 0.02 mag.

The IRAC data for the nearby T Tauri star TW Hya, a result of an earlier data release, were reduced separately using a different procedure. Fluxes were measured in a 10 pixel radius, with an outer radius of 20 pixels for sky subtraction (not important for this bright object).

### 3. Results

Table 1 lists the photometric results from IRAC, along with the dates of observation, positions measured from the IRAC images, and 2MASS magnitudes (Cutri et al. 2003) when available. Typical random errors in the photometry appear to be of order 0.02 - 0.03 mag, except for the faintest sources. As mentioned in the previous section, there may be systematic errors in the photometric zero points of  $\sim 0.05$  mag, but because these data were obtained during two campaigns, such systematic differences should apply relatively equally to all objects, and thus differential

magnitudes and colors among the Taurus stars should be slightly more reliable than absolute magnitudes.

### 3.1. IRAC [3.6] - [4.5] vs. [5.8] - [8] diagram and classification

Figure 1 shows that the [3.6] - [4.5] vs. [5.8] - [8] colors of the Taurus systems are concentrated in three fairly distinct regions. The densest cluster of data points reside near the origin, corresponding roughly to the nearly-zero colors expected for stellar photospheres in this wavelength region. A second reasonably well-defined set of measurements lies within [3.6] - [4.5]  $\sim$  0.2 – 0.7, [5.8] - [8]  $\sim$  0.6 – 1.0. A third, less well-defined (and much less populated) group of objects exhibits a similar range of [5.8] - [8] colors but much redder [3.6] - [4.5] colors.

This grouping of points in the [3.6] - [4.5] vs. [5.8] - [8] diagram is related to the presence of circumstellar dust. The principal classification scheme for pre-main sequence stars is the Class 0-I-II-III system, which characterizes objects in terms of their infrared excesses or spectral energy distributions (SEDs) (e.g., Lada & Wilking 1984; Adams, Lada, & Shu 1987; Andre, Ward-Thompson, & Barsony 1993, 2000). Class 0 and I objects are thought to be protostars surrounded by dusty infalling envelopes, and thus exhibit both relatively strong far-infrared emission and significant near-infrared extinction from their envelopes; Class II systems are stars with disks, and thus exhibit less infrared excess and near-infrared extinction (unless observed edge-on); and Class III objects are essentially stars without significant amounts of circumstellar dust (see §6 for further discussion). Based on this scheme, the open circles near the origin, having basically photospheric colors, should be Class III systems; the main body of stars with significant infrared excesses should be Class II (disk) systems; and the reddest objects in both colors should be Class 0-I systems.

We started our analysis by adopting the SED classifications given by KH95, which were based on combining ground-based photometry with IRAS fluxes. We revised the KH95 classifications in a few cases, for reasons described below. In addition, for some objects we made new classifications based on IRAC colors, to be consistent with the overall groupings which emerged from the original KH95 classifications.

We find that the 0-I-II-III SED classes generally account for the groupings seen in Figure 1, with a few discrepancies. The Class III sources (open circles) lie near the origin, with nearly zero colors, as expected; the Class II sources (filled circles) exhibit red colors consistent with excess (dust) emission; and the reddest systems are generally Class 0-I sources (open squares and triangles). The principal ambiguity occurs for Class I systems; three out of seven such systems shown in Figure 1 lie near the red end of the distribution of Class II systems, a result whose implications are discussed more fully in §6.

In a few cases the identification of a system as Class II or Class III is also ambiguous. Some T Tauri stars have holes in their inner disks; given the absence of disk dust close to the central star, such objects may have disks emitting at far-infrared etc. wavelengths, while exhibiting little

or no near- to mid-infrared excess emission. Thus the distinction between “Class II” and “Class III” may depend upon the wavelength of observation.

Two objects particularly illustrate this problem. The open circle with the reddest [5.8] - [8] color (= 0.205) in Figure 1 represents the star CoKu Tau 4. Recent IRS spectra from *Spitzer* show that this object has essentially no infrared excess from  $\sim 5 - 8\mu\text{m}$ , while exhibiting extremely large excess emission at wavelengths longward of  $20\mu\text{m}$ . This spectral energy distribution (SED) is most simply interpreted as that of a disk with a very optically thin or evacuated inner hole, and an effective disk edge (an optically-thick disk “wall”) at a radius  $\sim 10$  AU (Forrest et al. 2004; D’Alessio et al. 2005a).

The second illustrative object is TW Hya, whose position in the [3.6] - [4.5] vs. [5.8] - [8] diagram is denoted by a solid triangle. TW Hya has a SED that is fairly similar to that of CoKu Tau 4, and which has been interpreted in a similar manner as a disk system with an inner hole. The inner radius of the optically-thick disk wall is smaller in TW Hya than in CoKu Tau 4 ( $\sim 4$  AU), and there evidence for a small amount of dust inside the hole (Calvet et al. 2002). GM Aur also exhibits similar behavior (Rice et al. 2003; §5).

For these reasons, we have therefore identified systems as IRAC Class II or III (Table 1), based on the presence of significant excesses over photospheric levels *in the IRAC bands*. This means that the SED classifications differ in a few cases from those adopted by KH95. Specifically, unless there is a significant disk excess at  $8\mu\text{m}$ , we assign the object to IRAC Class III. In the case of CoKu Tau 4, even though it was assigned Class II by KH95, and has a small excess in the [8] band, we assign it to IRAC Class III as well, because it is much closer in its colors to the other Class III systems.

We find that the break in the distribution of colors at around [5.8] - [8]  $\sim 0.3 - 0.4$  corresponds accurately to the distinction between Classical T Tauri Stars (CTTS) and Weak Emission T Tauri Stars (WTTS) (Herbig & Bell 1988; White & Basri 2003). As discussed in more detail in §6, the CTTS exhibit disk accretion onto the central star, while the WTTS do not, and detectable accretion is generally accompanied by warm dust emission from the inner disk. This distinction is clear in our IRAC data. All of the CTTS (solid circles) are Class II, but not all of the WTTS (open circles) have previously been identified as Class III, i.e. some WTTS have outer disks and longer-wavelength excess dust emission. The prime example of this is CoKu Tau 4, which is a WTTS with a small  $\text{H}\alpha$  equivalent width of around  $2\text{ \AA}$  (Cohen & Kuhl 1979), indicating that there is very little if any accretion onto the central star. In this case, the emission class is more consistent with the assignment of IRAC SED Class (III) than with the previous Class II assignment by KH95. In contrast, TW Hya is a CTTS, accreting from its disk, with strong  $\text{H}\alpha$  emission and significant ultraviolet continuum excess radiation (Calvet et al. 2002; Muzerolle et al. 2000; Alencar & Batalha 2002); thus, it is not surprising that TW Hya has a much redder [5.8] - [8] color than CoKu Tau 4.

In general, the CTTS/II fall in a well-defined area of the color-color diagram. The only

exception, outside of TW Hya as described above, is 04301+2608. This object has  $[3.6] - [4.5] = 0.33$ , typical of other disk systems, but a very red long wavelength color,  $[5.8] - [8] = 1.67$ , consistent with the relatively bright IRAS fluxes observed (see §5). Briceño et al. (2002) noted the very low apparent luminosity of 04301+2608, given its M0 spectral type, and suggested that it might be an edge-on disk system with substantial contributions of scattered light at shorter wavelengths.

The open squares and triangles are objects identified as Class I systems by KH95, plus DG Tau B, which was not assigned a type by KH95. DG Tau B is extremely red in IRAC colors ( $[3.5] - [4.5] = 1.61$ ;  $[5.8] - [8] = 1.04$ ), and exhibits an extended bipolar nebulosity with a dark lane running across the middle seen at optical and near-infrared wavelengths similar to that observed for other Class I systems (e.g., Stapelfeldt et al. 1997; Padgett et al. 1999). Because at least some Class 0/I objects show extended nebulosities, we show photometry for Class I objects for both the standard aperture radius of 5 pixels (6 arcsec, corresponding to 840 AU at the 140 pc distance of Taurus), plus the standard aperture corrections noted above for a point source, as well as a “large aperture” measurement with an aperture of 10 pixels (12 arcsec, 1680 AU). The results for the differing apertures are almost identical except for IRAS 04368+2557, which is the driving source for the molecular outflow in L1527. This system is classified by André et al. (2000) as a borderline Class 0/I system, whereas Chen et al. (1995) identify it as a Class 0 system. The relatively blue color in  $[5.8] - [8]$  for this object is likely due to the wings of the  $10\mu\text{m}$  silicate feature affecting the flux in the  $[8]$  band, with a long-wavelength cutoff of about  $9.3\mu\text{m}$ . IRAS 04368+2557 appears as a very large, extended nebulosity without a central point source in all the IRAC bands. These images will be discussed in a forthcoming publication (Allen et al. 2005).

One object, HV Tau C, has colors almost equal to those of the Class I source 04260 + 2642, while exhibiting a large  $\text{H}\alpha$  equivalent width consistent with it being a CTTS (White & Ghez 2001). (HV Tau AB itself is a WTTS/Class III close binary.) Optical and near-infrared imaging of HV Tau C shows a dark lane consistent with absorption in a flattened circumstellar disk seen nearly edge-on (Monin & Bouvier 2000; Stapelfeldt et al. 2003). However, Stapelfeldt et al. (2003) concluded that a dusty envelope appears to be required in addition to a disk in order to explain the observations. This suggests that HV Tau C might actually be a Class I source, with a relatively tenuous infalling envelope in addition to a circumstellar disk (see §6).

The crosses in Figure 1 denote systems with spectral types later than M6, and are thus identified as probable brown dwarfs (Luhman 1999). Specifically, these objects are GM Tau (M6.5, White & Basri 2003); KPNO 4, 5, 6, 7 (M9.5, M7.5, M8.5, M8.25, respectively, Briceño et al. 2002); and IRAS 04414+2506 (M7.25, Luhman 2004). Of the six such objects observed so far, four have clear IRAC excesses indicating the presence of disks – and consistent with the colors of disks of higher-mass T Tauri stars – while one (KPNO 5) clearly exhibits photospheric colors. The small  $[5.8] - [8]$  excess exhibited by the M9.5 star KPNO4 should be discounted because of large photometric errors for this faint object (Table 1). Although Briceño et al. (2002) estimated a large  $\text{H}\alpha$  equivalent width suggestive of disk accretion in KPNO4, a more recent high-resolution study (Muzerolle et al. 2003) indicates a much lower equivalent width, with marginal evidence of accretion

from the  $H\alpha$  profile. This system probably is not accreting from a circumstellar disk.

In Figure 1 we also show the reddening vectors for a Vega-like spectrum and  $A_V = 30$ , estimated from interpolating the Mathis (1990) extinction law, applying this law to a model of the photospheric emission of Vega, and integrating the resultant spectrum over the IRAC bandpasses. The effect of circumstellar disk emission is to distribute the sources redward in both colors; in contrast, circumstellar extinction is predicted to move sources much more vertically, or even slightly blueward in the [5.8] - [8] color, due to the effect of the 10  $\mu\text{m}$  silicate feature on the IRAC [8] band as mentioned above. In contrast, systems with strong disk emission tend to be much redder in [5.8] - [8]; many CTTS exhibit silicate features in emission, producing a color shift distinct from circumstellar absorption. Thus it appears that the [3.6] - [4.5] vs. [5.8] - [8] diagram can be especially useful for distinguishing disk emission from the effects of interstellar absorption.

### 3.2. Other color-color diagrams

Figure 2 shows the [3.6] - [4.5] vs. [4.5] - [5.8] diagram. The general distribution of points into the three main groups is more or less the same as in Figure 1, although the division between C/Class II and W/Class III systems is less well defined. Such a diagram may be useful in many star-forming regions, where the sensitivity in band [8] is reduced by bright extended emission attributed to Polycyclic aromatic Hydrocarbons (PAH).

Figure 3 shows other color-color diagrams using the shortest IRAC bands, which have the highest sensitivity and are least affected by PAH emission, with near-infrared colors taken from the 2MASS point source catalog. If the true reddening vectors are reasonably well-represented by the values adopted here, then it appears that combinations of deep near-infrared measurements and IRAC data can be used to distinguish between stars with and without circumstellar dust emission (i.e., between Class III and Class II/I/0 systems). The  $H - [3.6]$  vs. [3.6] - [4.5] diagram appears to provide a particularly clean break, at least for systems similar to those of the Taurus star-forming region.

D’Alessio et al. (1999) used the ground-based and IRAS data listed in KH95 to construct a “median” spectral energy distribution or SED for Taurus Class II stars of spectral type K5-M2. Because many Taurus stars in this spectral type range are yet to be observed with IRAC, we defer the construction of a similar median SED to a later paper. Here we make a preliminary estimate of the consistency of the median SED with the observed colors of the sample so far. We do this by taking the fluxes of the median SED from D’Alessio et al. (1999) and interpolating linearly in log flux vs. log wavelength, and then convolving the resulting spectrum with the predicted transmissions of the IRAC bands (Fazio et al. 2004) Because the ground-based data are sparsely sampled in the IRAC range (most objects have only K,L, and N magnitudes, with few M magnitudes), this procedure is relatively crude, but serves as an initial consistency check. We thus estimate the following IRAC colors for the median SED; [3.6] - [4.5] = 0.40, [4.5] - [5.8] = 0.52, and [5.8] - [8]

= 0.83. As can be seen from the figures, these colors lie near the middle of the distribution of CTTS or Class II colors, indicating reasonable agreement, though the predicted [4.5] - [5.8] color is a bit redder than typical.

#### 4. Comparison with models

Figure 4 compares two of the main IRAC color-color diagrams with models for Class I and II systems. The disk models shown are from the most recent calculations by D’Alessio et al. (2005b), which include dust settling in the upper disk layers, and a more refined treatment of the emission of the wall at the dust sublimation radius, which takes into account the optically thin layers of the wall atmosphere. The models are coded by color for the logarithm of the disk mass accretion rate in units of solar masses per year, with  $\dot{M} = -7$  (blue),  $-8$  (green), and  $-9$  (red). At a fixed accretion rate, models are shown for two values of the inclination angle,  $\cos i = 0.5$  and  $0.86$ , and values of the dust depletion parameter  $\epsilon = 1, 0.1, 0.01, \text{ and } 0.001$  (see D’Alessio et al. 2005b).<sup>1</sup>

The disk models reproduce the range of observed IRAC colors very well at accretion rates spanning the expected values for Taurus systems (e.g., Gullbring et al. 1998, Hartmann et al. 1998). The current IRAC sample has only a modest number of objects in common with the Gullbring et al. and Hartmann et al. accretion rate measurements; therefore, we cannot say with confidence whether the detailed colors of individual objects are consistent with model predictions given their measured mass accretion rates. We will make a more detailed test of the model predictions when the Taurus survey data are complete.

The Class I models are taken from Allen et al. (2004) for two luminosities,  $1 L_{\odot}$  (magenta lines) and  $0.1 L_{\odot}$  (red lines), and two values of the centrifugal radius  $R_c$  of 50 AU (solid line) and 300 AU (dashed line); Values for the density scaling parameter  $\rho_1$  increase from bottom to top along a given line, with markers (solid squares) at values of  $\log \rho_1 = -14, -13.5, \text{ and } -13$ .<sup>2</sup> These parameters have been found to span the characteristic range needed to explain Taurus Class I SEDs including IRAS fluxes (Kenyon, Calvet, & Hartmann 1993 = KCH93).

The models predict that objects with low mass infall rates and/or large centrifugal radii will have colors similar to that of “pure disk” systems. While the protostellar envelope models generally span the range of observed colors for reasonable parameters, it is difficult to match the detailed parameters estimated by KCH93 for individual objects with these models. The reason is that inferred parameters are very sensitive to the assumed geometry, as discussed further in §6.

---

<sup>1</sup>The parameter  $\epsilon$  denotes the factor by which the dust in upper layers of the disk is depleted from the standard value.

<sup>2</sup> $R_c$  is the outer radius at which envelope material falls onto the disk due to the angular momentum barrier;  $\rho_1$  is the density the infalling envelope would have at 1 AU if  $R_c \rightarrow 0$  (see Kenyon, Calvet, & Hartmann 1993 for further discussion). For a mass infall rate of  $10^{-5} M_{\odot} \text{ yr}^{-1}$  to a  $1 M_{\odot}$  protostar,  $\rho_1 \sim 5 \times 10^{-14} \text{ g cm}^{-3}$ ;  $\rho_1 \propto \dot{M}_{*}^{-1/2}$ .



## 5. Spectral Energy Distributions

Figures 5 et seq. display SEDs for our program sample. The SEDs are constructed from the IRAC data, 2MASS JHK photometry, and when available, other photometry listed in KH95. In many panels we show the median CTTS SED of D’Alessio et al. (1999), approximately scaled by eye to the observed infrared fluxes, along with the long-wavelength colors of the K7 WTTS/Class III star V819 Tau. Our purpose in including these comparison SEDs is merely to provide a standard reference in most panels for making rough intercomparisons between systems, without making extinction corrections. There has been no attempt to make detailed fits, which would require careful analysis of spectral types and optical colors to make the necessary reddening corrections.

In general, there is good agreement with ground-based data. The Class I systems show a variety of behavior. The most heavily-reddened systems show evidence of silicate absorption, as expected. Among the Class II systems, many exhibit disk SEDs comparable to that of the median SED, such as CX Tau, FV Tau/c, DF Tau, IQ Tau, DS Tau, etc. A few objects exhibit disk emission that falls off faster to longer wavelengths than the median SED (e.g., CIDA 8, 11, 12, 14, DK Tau 1, and possibly JH 223). DR Tau shows a very large excess consistent with strong accretion heating (e.g., Bertout, Basri, & Bouvier 1988). One peculiar result is that the apparent 2MASS magnitudes for CIDA 9 are extremely inconsistent with the JHK magnitudes from KH95; the latter are much more consistent with the IRAC colors. UZ Tau W (UZ Tau Ba + Bb; White & Ghez 2001) also poses a problem for analysis, because the 2MASS H and  $K_s$  magnitudes are about 0.7 and 0.8 mag brighter, respectively, than those listed by KH95 (see Figure 6), which produces a very large uncertainty in assessing the level of infrared excess. The KH95 magnitudes are more consistent with the White & Ghez (2001) K magnitude for UZ Tau W as well as with the IRAC results. UZ Tau EW, with a separation of 3.5 arcsec, is poorly resolved by 2MASS, which may be the source of the discrepancy.

GM Aur is a CTTS with a small IRAC excess but much larger excesses at  $\lambda \geq 10\mu\text{m}$  (Rice et al. 2003), similar in many respects to the CTTS TW Hya and the WTTS CoKu Tau 4, as discussed above. KH95 identified DI Tau as a Class II object, citing a  $10\mu\text{m}$  excess with a very large error, whereas we find no evidence for excesses out to band [8], and thus identify it as Class III. Meyer et al. (1997) detected no  $10\mu\text{m}$  excess based on detailed ground-based data; IRAS emission in the region of this source is dominated by the nearby CTTS DH Tau, and thus whether any excess is present at long wavelengths is currently uncertain.

The WTTS systems LkHa332 G1 and G2 have no IRAC excesses; thus we identify both as Class III systems, in contrast to the Class II given by KH95 for G1. The IRAS fluxes in the region are consistent with arising entirely from LkHa 332 = V955 Tau. We find excess emission from UZ Tau w, in contrast to the Class III identification in KH95, but consistent with the large H $\alpha$  equivalent widths of this close binary system found by Hartigan & Kenyon (2003).

Our small sample of brown dwarfs with disks have colors similar to those of higher-mass CTTS. This is undoubtedly because the disk emission is optically thick, and geometrical properties of the

disks are relatively unimportant in the IRAC range, i.e. the disks are thought to be geometrically flat except possibly at the inner edge of the dust disk (see, e.g. Dullemond Dominik & Natta 2001; Luhman et al. 2005).

## 6. Discussion

One of the purposes of conducting this survey of Taurus is to investigate how reliably objects can be classified using IRAC colors by reporting results for well-known, independently-classified systems. As mentioned in §3.1, the major system of infrared classification depends upon an infrared spectral index, typically measured from about  $1 - 2\mu\text{m}$  to about  $10 - 20\mu\text{m}$  (Lada & Wilking 1984; Adams et al. 1987). Plotted as  $\log \lambda F_\lambda$  vs.  $\log \lambda$ , Class 0/I systems have positive spectral indices, indicating substantial circumstellar envelopes and are usually thought to be protostars (Adams et al. 1987, André, Ward-Thompson, & Barsony 1993). Class II sources have negative slopes, but far less steep than that of a Rayleigh-Jeans spectrum, and are identified as systems with dusty circumstellar disks (Lynden-Bell & Pringle 1974; Adams et al. 1987; Kenyon & Hartmann 1987); and Class III systems have steep negative slopes consistent with those expected for a (reddened) stellar photosphere, essentially a Rayleigh-Jeans slope (Lada & Wilking 1984; Adams et al. 1987).

The other system for classifying low-mass pre-main sequence stars, as previously mentioned in §3.1, depends upon spectroscopic criteria, introduced by Herbig & Bell (1988) and refined by White & Basri (2003). Using criteria based on  $\text{H}\alpha$  emission - usually a spectral-type-dependence of equivalent width, correlated in some cases by velocity width - one may divide systems into “Classical” T Tauri stars or CTTS vs. “Weak” T Tauri stars or WTTS. The WTTS have relatively weak  $\text{H}\alpha$  equivalent widths, and narrow  $\text{H}\alpha$  line profiles produced by chromospheric activity; the CTTS have larger  $\text{H}\alpha$  emission and broader profiles thought to be produced by disk accretion (see discussion in Hartmann 1998).

We have shown that IRAC colors can be used to classify systems accurately between CTTS and WTTS. This is not surprising, given that accretion onto the central star has been known to correlate with infrared excess emission in the  $L$  photometric band (Hartigan et al. 1990). Basically, it appears that all systems with detectable gaseous accretion onto the central star (through *either* ultraviolet continuum excesses or broad  $\text{H}\alpha$  profiles) have enough small dust particles carried along with the accreting gas to provide significant near-infrared excess emission. Whether a system should be identified as Class II or Class III is more complicated, depending upon whether the disk has an inner hole. We have skirted this issue of nomenclature in this paper by defining systems based on the presence or absence of excesses in the IRAC bands.

The agreement between the observed Taurus colors and the current disk models is encouraging. These model predictions are very similar to those presented in Allen et al. (2004) and Megeath et al. (2004). The Taurus results suggest that the methods used in the above papers are adequate for identifying Class II/CTTS in star-forming regions, with appropriate allowances for extinction.

The disk models predict that the IRAC colors get redder as the mass accretion rate increases, although inclination and dust properties also contribute in a complicated manner. A preliminary investigation of [3.6] - [4.5] vs. mass accretion rates from the literature is not conclusive, given the small number of systems with accretion rates in our current sample; we will revisit this question when the Taurus survey is complete.

The disk models of Whitney et al. (2004) do not strongly populate the region of CTTS/Class II sources found observationally here. As Whitney et al. note, this is likely because they have few models appropriate for low-mass stars. The protostellar envelope models of Whitney et al. similarly do not show colors corresponding to L1527, but this may be due to the relatively small aperture we used for the photometry of this object considering the spatial extension of its emission (Allen et al. 2005).

We also find that our small sample of Taurus Class I systems tend to divide into two comparably-sized groups; one that is very much redder than Class II systems, and another that exhibits IRAC colors which are similar to the reddest Class II objects (§3.1). Using the Class 0-I criteria to distinguish protostellar systems from Class II/T Tauri systems implicitly depends on protostellar envelopes having significant opacity in the IRAC bands, especially along the line of sight to the central (proto)star; otherwise the envelope can neither absorb much light or produce much emission in the IRAC bands. The extinction produced by an infalling protostellar envelope depends upon the infall rate, the angular momentum of the infalling material, the size of envelope holes driven by outflows, and departures from sphericity of the initial protostellar core, along with the system inclination to the line of sight (Adams et al. 1987; KCH93; Calvet et al. 1994; Hartmann, Boss, & Calvet 1996; Whitney et al. 2003).

It is instructive to make a simple estimate of envelope optical depth in the IRAC region, ignoring complicating geometric factors for the moment. Assuming a spherical envelope in steady free-fall at mass infall rate  $\dot{M}$  towards a central protostar of mass  $M_*$ , the radial mass column density is

$$\int_{r_0}^{\infty} dr \rho = \frac{\dot{M}}{2\pi(2GM_*)^{1/2}r_0^{1/2}}, \quad (1)$$

where  $r_0$  is the inner radius. If we identify  $r_0$  as comparable to the centrifugal radius, i.e. roughly the radius at which material falls out onto the disk, we can then make an estimate of the envelope optical depth as a function of this parameter. Using Draine & Lee (1984) opacities at  $\lambda = 3.4\mu\text{m}$ , we find numerically

$$\tau(3.4\mu\text{m}) \sim 1 \left( \frac{\dot{M}}{4 \times 10^{-6}M_{\odot} \text{yr}^{-1}} \right) \left( \frac{M}{0.5M_{\odot}} \right)^{-1/2} \left( \frac{r_0}{100\text{AU}} \right)^{-1/2}. \quad (2)$$

The fiducial value  $\dot{M} = 4 \times 10^{-6}M_{\odot} \text{yr}^{-1}$  is the typical infall rate for Taurus Class I sources deduced by KCH93, based mostly on the analysis of longer-wavelength IRAS fluxes. KCH93 also estimated centrifugal radii (comparable to  $r_0$ ) of 70-300 AU for most systems, although with con-

siderable uncertainty. For lower values of envelope column density ( lower values of  $\dot{M}r_o^{-1/2}$ ), the envelope will be essentially transparent at IRAC wavelengths, while higher values of envelope column density will result in potentially significant effects of the envelope in extinguishing the central source and producing extra dust emission. Thus, it is not very surprising that (of our small sample), four of the Class 0/I sources have IRAC colors significantly different from those of Class II (disk) systems (04368+2557, 04365+2535, 04381+2540, DG Tau B) while three Class I systems exhibit colors at the red end of the disk systems (04260+2642, 04248+2612, 04489+3042). We suggest that many or most Class I systems with infall rates similar to or larger than those typical of Taurus should exhibit distinct IRAC colors from those of Class II systems.

The above estimate neglects the uncertainties that can arise in classifying individual systems due to additional departures from sphericity in the envelope, such as bipolar outflow holes or collapsing flattened envelopes (e.g., Hartmann et al. 1996). To expand upon this, we note that of the sources in common with those modelled by KCH93, the reddest systems in [3.6] - [4.5] (04368+2557, 04365+2535, and 04381+2540) had relatively high values of the density scaling parameter  $\rho_1$ , consistent with the IRAC observations. Conversely, the 04489+3042 system is bluer in [3.6] - [4.5] and had a low  $\rho_1$  according to the modelling of KCH93. The system 04248+2612 has relatively blue colors, even though KCH93 found a high value of  $\rho_1$  in their fitting. However, the fit of KCH93 adopted a large value of  $R_c = 300$  AU and a very low viewing inclination  $i = 10^\circ$ , and both parameter choices reduce the line-of-sight column density in these rotating collapse models. These results illustrate but probably underestimate the sensitivity of the IRAC colors to protostellar envelope geometry, because they do not include bipolar outflow holes. Viewing a highly embedded protostellar source along an evacuated cavity could easily produce IRAC colors determined entirely by the disk properties of the system.

Alternatively, one might ask whether the Class I group with similar colors as Class II systems might not simply be identified Class II as well. Chiang & Goldreich (1999) suggested that many objects identified as Class I might really be Class II, i.e. they disk systems seen more nearly edge-on; White & Hillenbrand (2004) recently made a similar suggestion. A problem with this idea is that edge-on disks do not necessarily, or even naturally, exhibit the same SEDs and colors as Class I envelope systems. As discussed by D’Alessio et al. (1999) in some detail, because T Tauri disks are thought to be very optically thick, the observed SED is extremely sensitive to the inclination of observation. As shown in Figure 13 of D’Alessio et al. (1999), which shows the predicted spectrum of a disk model at different viewing angles, there is only a small range of inclinations for which the SED is roughly comparable to that of Class I systems. Slightly more pole-on, the SED looks like that of a normal Class II object; slightly more edge-on, huge silicate absorption is predicted.

In our sample of Class I systems, the group with nearly “Class II colors” does not exhibit the blue [5.8] - [8] color one would expect for deep silicate absorption, nor is such absorption apparent in ground-based data (e.g., Figure 5), and so these systems are unlikely to be explained as purely edge-on disks. Note that the HV Tau C system, whose image clearly shows absorption from a nearly edge-on disk, shows no evidence for strong silicate absorption from the [5.8] - [8.0] color; however,

as noted in §3, Stapelfeldt et al. (2003) concluded that an extended dusty envelope probably must be included along with a disk to explain the near-infrared scattered light image, and this dust could in principle provide compensating silicate feature emission. Stapelfeldt et al. showed that the infall rate for such an envelope would be quite low,  $\sim 10^{-7}M_{\odot}\text{yr}^{-1}$ , suggesting that this object may be in transition between Class I and Class II.

D’Alessio et al. (1999) also pointed out that edge-on Class II disk systems should appear to be underluminous, by roughly an order of magnitude. The three Class I systems with colors comparable to the reddest Class II objects, 04260+2642, 04248+2612, and 04489+3042, have apparent bolometric luminosities of 0.09, 0.36, and  $0.3L_{\odot}$  respectively (KH95). Hubble Space Telescope images of 04260+2642 indicate that it is an edge-on disk system (Stapelfeldt 2005, personal communication), consistent with its relatively low luminosity (D’Alessio et al. 1999). The other two objects have luminosities only marginally below the median luminosity of Class I systems in Taurus (KH95). Furthermore, 04248+2612 has a well-observed, extended near-infrared reflection nebulosity typical of Class I systems (Lucas & Roche 1997; Padgett et al. 1999; Park & Kenyon 2002), and NICMOS observations at  $1.1\ \mu\text{m}$  using *Hubble Space Telescope* also show extended nebulosity around 04489+3042 in a pattern much more similar to that of envelope than edge-on disk systems (L. Hartmann, unpublished). We conclude that 04248+2612 and 04489+3042 are likely to be true Class I systems.

To make more progress in understanding the properties (or even existence) of protostellar envelopes, inclusion of longer-wavelength data is crucial. Comprehensive observations of a range of Class I systems with IRAC, IRS, and MIPS should yield significant new insights into protostellar evolution.

## 7. Conclusions

We have presented results from a survey of 82 Taurus pre-main sequence stars as observed with the IRAC camera on *Spitzer* Space Telescope. These data provide the first indication of the presence or absence of infrared excesses in the 3-8  $\mu\text{m}$  range for about half of our sample, and add considerably to our knowledge of the SEDs of many more systems. The results generally confirm the color classification scheme used in previous IRAC studies of star-forming regions. The predictions of disk and protostellar envelope models are consistent with the observed IRAC colors, and suggest a relatively clear difference in between stars with and without optically-thick disks. Among systems with disks, we find a very strong correlation of IRAC excesses with the presence of accretion. Our results should be of use for testing more detailed models of disks and envelopes in pre-main sequence systems, and for interpreting IRAC observations of more distant, less well-studied star-forming regions.

We thank the referee, Karl Stapelfeldt, for useful comments and for communicating new results. This work is based on observations made with the *Spitzer* Space Telescope, which is operated by the

Jet Propulsion Laboratory, California Institute of Technology, under NASA contract 1407. This work was supported in part through contract 1256790 issued by JPL/Caltech. The research of L.H. and N.C. was supported in part by NASA grants NAG5-9670, NAG5-13210, NAG5-10545, and grant AR-09524.01-A from the Space Telescope Science Institute. K.L. was supported by grant NAG5-11627 from the NASA Long-Term Space Astrophysics program.

## REFERENCES

- Adams, F. C., Lada, C. J., & Shu, F. H. 1987, *ApJ*, 312, 788
- Alencar, S. H. P. & Batalha, C. 2002, *ApJ*, 571, 378
- Allen, L. E., et al. 2004, *ApJS*, 154, 363
- Allen, L. E., et al. in preparation
- Andre, P., Ward-Thompson, D., & Barsony, M. 1993, *ApJ*, 406, 122
- Andre, P., Ward-Thompson, D., & Barsony, M. 2000, in *Protostars and Planets IV*, eds. Mannings, V., Boss, A.P., & Russell, S. S. (Tucson: University of Arizona Press), 59
- Bertout, C., Basri, G., & Bouvier, J. 1988, *ApJ*, 330, 350
- Briceño, C., Calvet, N., Gomez, M., Hartmann, L. W., Kenyon, S. J., & Whitney, B. A. 1993, *PASP*, 105, 686
- Briceño, C., Luhman, K. L., Hartmann, L., Stauffer, J. R., & Kirkpatrick, J. D. 2002, *ApJ*, 580, 317
- Calvet, N., D'Alessio, P., Hartmann, L., Wilner, D., Walsh, A., & Sitko, M. 2002, *ApJ*, 568, 1008
- Calvet, N., Hartmann, L., Kenyon, S. J., & Whitney, B. A. 1994, *ApJ*, 434, 330
- Chen, H., Myers, P. C., Ladd, E. F., & Wood, D. O. S. 1995, *ApJ*, 445, 377
- Chiang, E. I. & Goldreich, P. 1999, *ApJ*, 519, 279
- Cohen, M. & Kuhl, L. V. 1979, *ApJS*, 41, 743
- Cutri, R.M., Skrutskie, M.F., van Dyk, S., & 25 more coauthors, *VizieR On-line Data Catalog*, 2246
- D'Alessio, P., Calvet, N., & Hartmann, L. 2001, *ApJ*, 553, 321
- D'Alessio, P., et al. 2005a, *ApJ*, in press

- D'Alessio, P., Calvet, N., Hartmann, L., & Franco-Hernandez, R., Sitko, M., & Servin, H. 2005b, in preparation
- Draine, B. T. & Lee, H. M. 1984, *ApJ*, 285, 89
- Dullemond, C. P., Dominik, C., & Natta, A. 2001, *ApJ*, 560, 957
- Fazio, G. G., et al. 2004, *ApJS*, 154, 10
- Forrest, W. J., et al. 2004, *ApJS*, 154, 443
- Gullbring, E., Hartmann, L., Briceño, C., & Calvet, N. 1998, *ApJ*492, 323
- Hartigan, P., Hartmann, L., Kenyon, S. J., Strom, S. E., & Skrutskie, M. F. 1990, *ApJ*, 354, L25
- Hartigan, P. & Kenyon, S. J. 2003, *ApJ*, 583, 334
- Hartmann, L. 1998, *Accretion Processes in Star Formation*, Cambridge University Press
- Hartmann, L., Calvet, N., & Boss, A. 1996, *ApJ*, 464, 387
- Hartmann, L., Calvet, N., Gullbring, E., & D'Alessio, P. 1998, *ApJ*, 495, 385
- Herbig, G. H. & Bell, K. R. 1988, *Lick Observatory Bulletin*, Santa Cruz: Lick Observatory, 1988; 1995, *VizieR Online Data Catalog*, 5073, 0
- Kenyon, S. J., Calvet, N., & Hartmann, L. 1993, *ApJ*, 414, 676
- Kenyon, S.J., & Hartmann, L. 1995, *ApJS*, 101, 117
- Lada, C. J. & Wilking, B. A. 1984, *ApJ*, 287, 610
- Landsman, W. B. 1993, in *ASP Conf. Ser. 52, Astronomical Data Analysis Software and Systems II*, ed. R. J. Hanisch, R. J. V. Brissenden, & J. Barnes (San Francisco: ASP), 246
- Luhman, K. L. 1999, *ApJ*, 525, 466
- Luhman, K. L. 2004, *ApJ*, 617, 1216
- Luhman, K. L., D'Alessio, P., Calvet, N., Allen, L. E., Hartmann, L., Megeath, S. T., Myers, P. C., & Fazio, G. G. 2005, *ApJ*, 620, L51
- Mathis, J. S. 1990, *ARA&A*, 28, 37
- Megeath, S. T., et al. 2004, *ApJS*, 154, 367
- Meyer, M. R., Beckwith, S. V. W., Herbst, T. M., & Robberto, M. 1997, *ApJ*, 489, L173
- Monin, J.-L., & Bouvier, J. 2000, *A&A*, 356, L75

- Muzerolle, J., Calvet, N., Briceño, C., Hartmann, L., & Hillenbrand, L. 2000, *ApJ*, 535, L47
- Muzerolle, J., Calvet, N., Hartmann, L., & D'Alessio, P. 2003, *ApJ*, 597, L149
- Padgett, D. L., Brandner, W., Stapelfeldt, K. R., Strom, S. E., Terebey, S., & Koerner, D. 1999, *AJ*, 117, 1490
- Park, S. & Kenyon, S. J. 2002, *AJ*, 123, 3370
- Rice, W. K. M., Wood, K., Armitage, P. J., Whitney, B. A., & Bjorkman, J. E. 2003, *MNRAS*, 342, 79
- Stapelfeldt, K.R. et al. 1997, in *IAU Symp. 182, Herbig-Haro Flows and the Birth of Stars*, ed. B. Reipurth & C. Bertout (Dordrecht: Kluwer), 355
- Stapelfeldt, K. R., Ménard, F., Watson, A. M., Krist, J. E., Dougados, C., Padgett, D. L., & Brandner, W. 2003, *ApJ*, 589, 410
- White, R. J. & Basri, G. 2003, *ApJ*, 582, 1109
- White, R. J. & Ghez, A. M. 2001, *ApJ*, 556, 265
- White, R.J., & Hillenbrand, L.A. 2004, *ApJ*, 616, 998
- Whitney, B. A., Indebetouw, R., Bjorkman, J. E., & Wood, K. 2004, *ApJ*, in press
- Whitney, B. A., Wood, K., Bjorkman, J. E., & Cohen, M. 2003, *ApJ*, 598, 1079



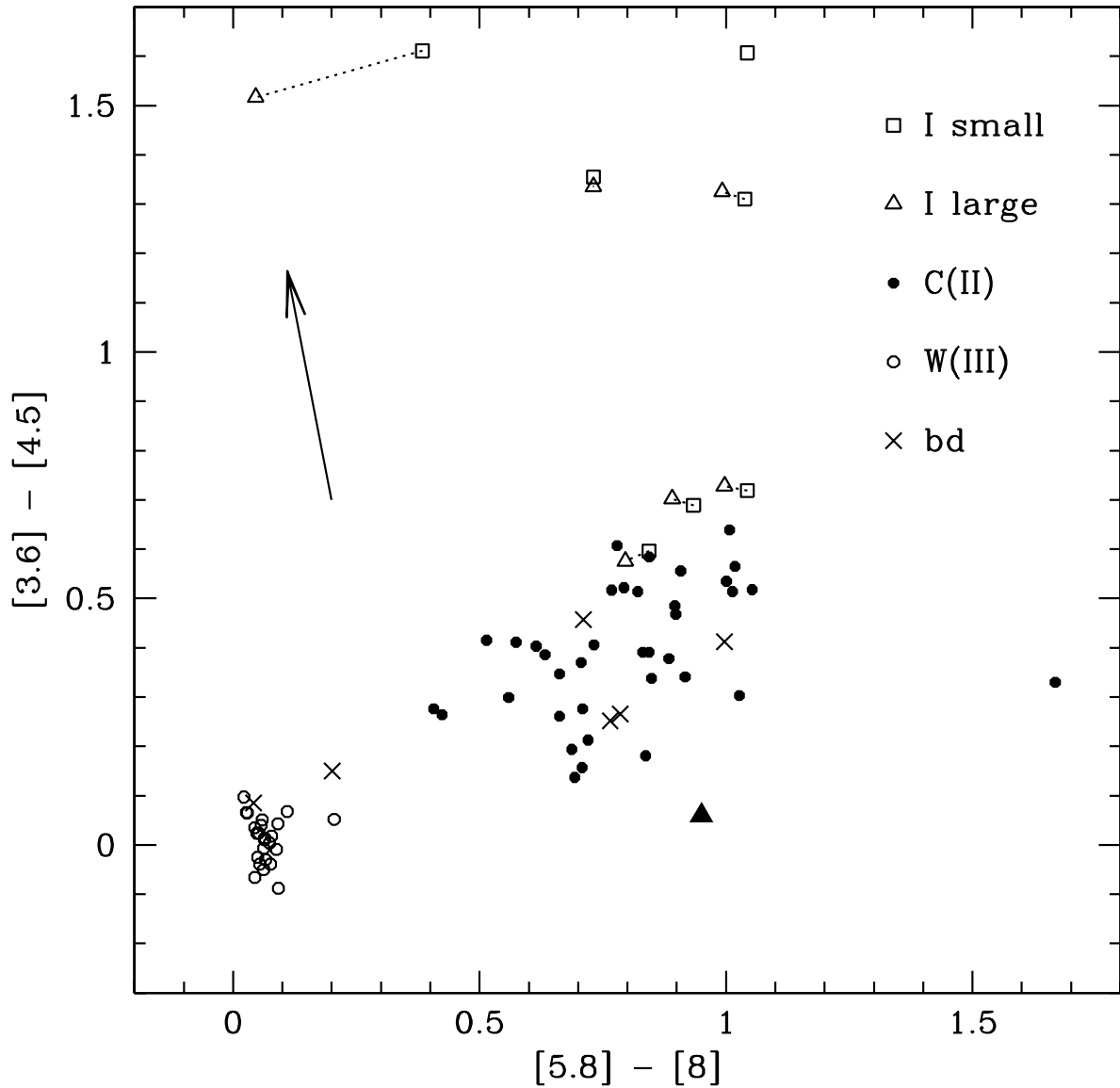


Fig. 1.— Color-color plot for the four IRAC bands. Open circles are WTTS/Class III objects, filled circles are CTTS/Class II systems, and open squares and triangles are Class 0/I systems measured in large and small apertures (see text for explanation). The crosses are brown dwarfs, and the solid triangle is TW Hya. Reddening vectors for  $A_V = 30$  are shown for the case of a Vega-like spectrum and the reddening law listed by Mathis (1990).

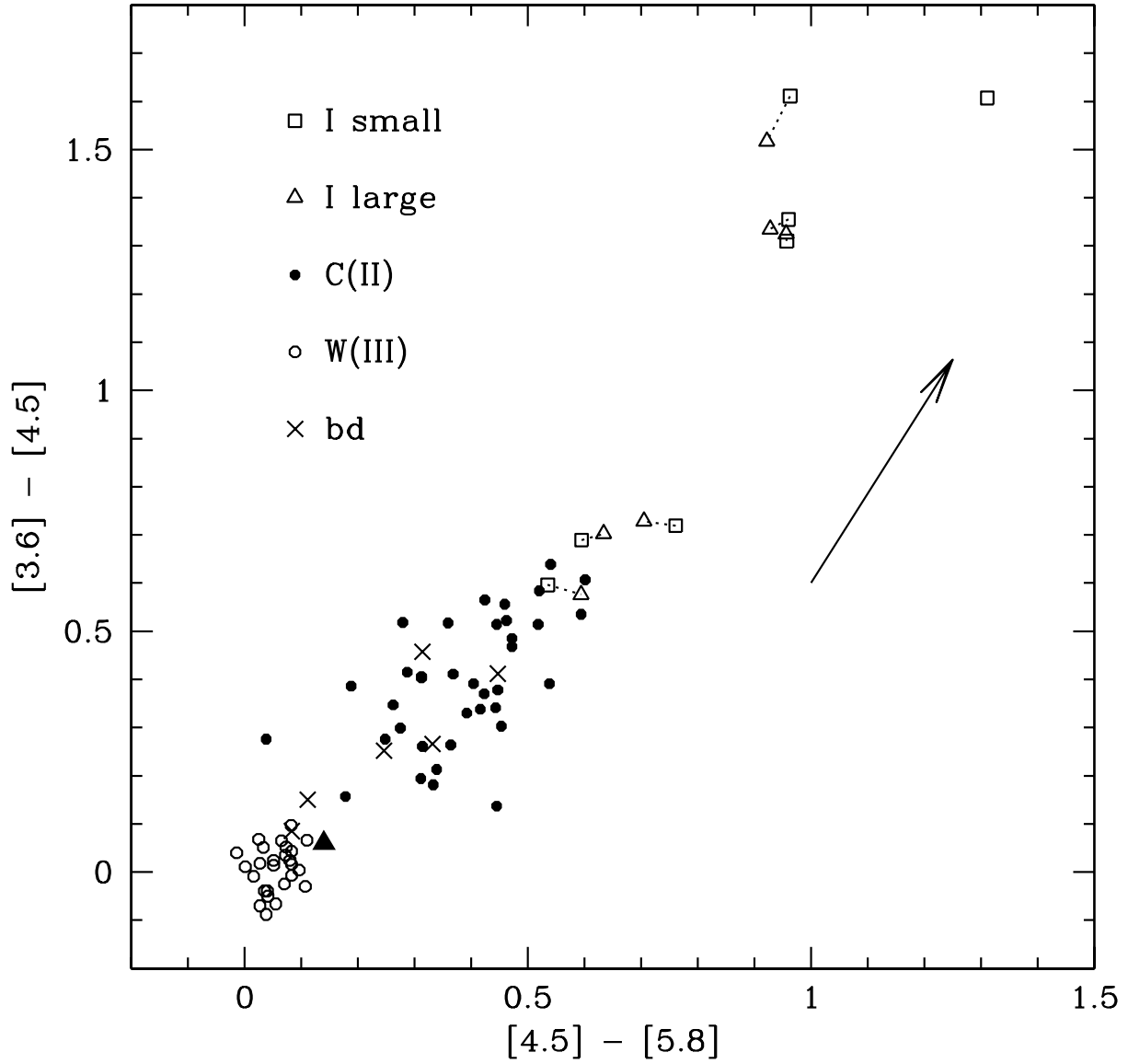


Fig. 2.— Alternative IRAC color-color plot, eliminating the longest-wavelength band. Symbols are the same as in Figure 1.

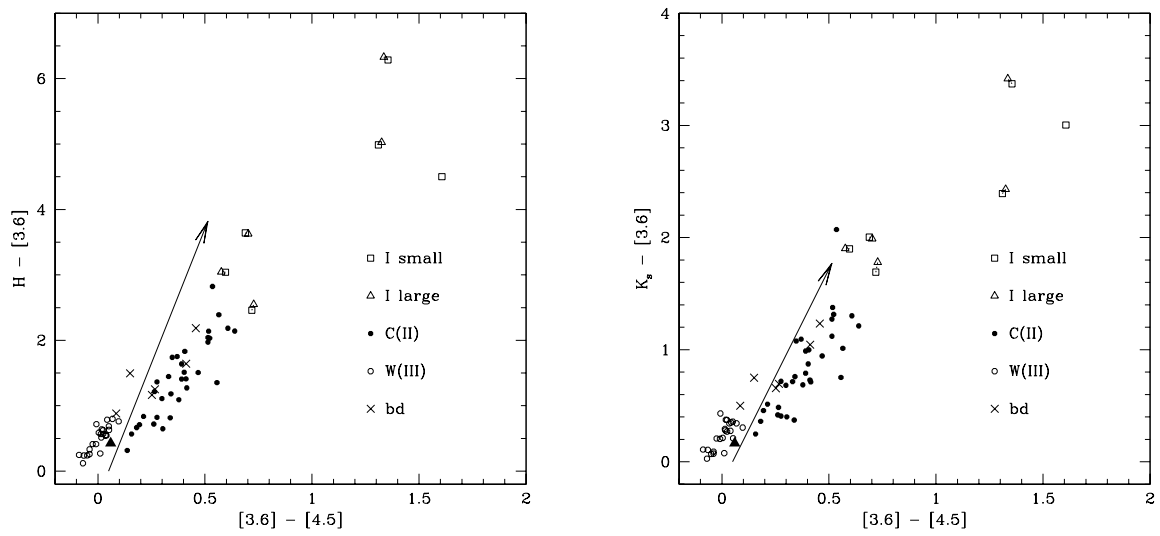


Fig. 3.— Color-color plots using near-infrared 2MASS magnitudes and the shortest-wavelength IRAC bands.

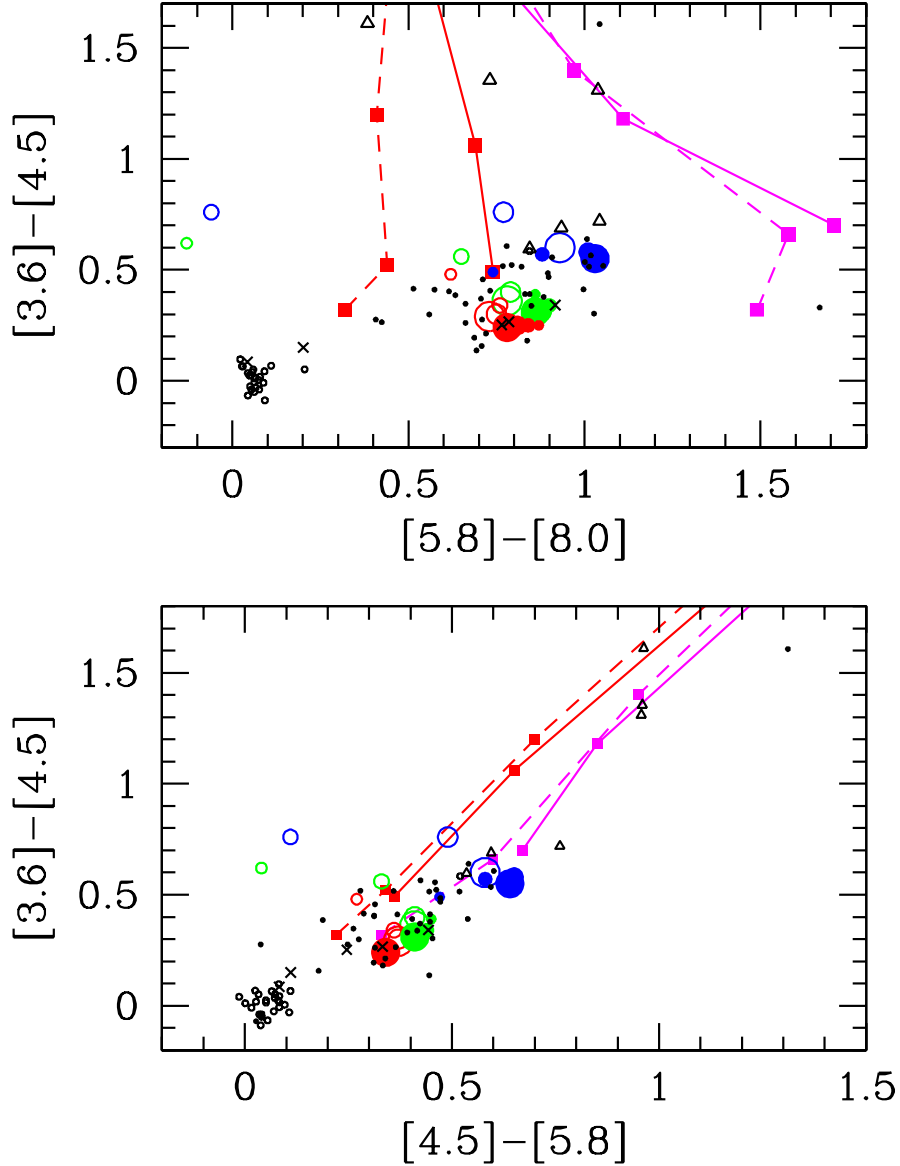


Fig. 4.— Comparison of observed and model colors. The data are shown in black, with symbols as in Figures 1 and 2. Class I models are taken from Allen et al. (2004) for two luminosities,  $1 L_{\odot}$  (magenta lines) and  $0.1 L_{\odot}$  (red lines), and two values of the centrifugal radius  $R_c$  of 50 AU (solid line) and 300 AU (dashed line). Values for the density scaling parameter  $\rho_1$  increase from bottom to top along a given line, with markers (solid squares) at values of  $\log \rho_1 = -14, -13.5,$  and  $-13$ . Disk model colors are taken from D’Alessio et al. (2005b) and are shown for values of the log of the mass accretion rate  $\log \dot{M} = -7$  (blue),  $-8$  (green), and  $-9$  (red). Disk models are shown for two values of the inclination angle,  $\cos i = 0.5$  (solid circles) and  $0.86$  (open circles), and for four values of the depletion parameter,  $\epsilon = 1, 0.1, 0.01,$  and  $0.001$  (D’Alessio et al. 2005b), labeled by symbol size; the smallest size corresponds to  $\epsilon = 1$ .

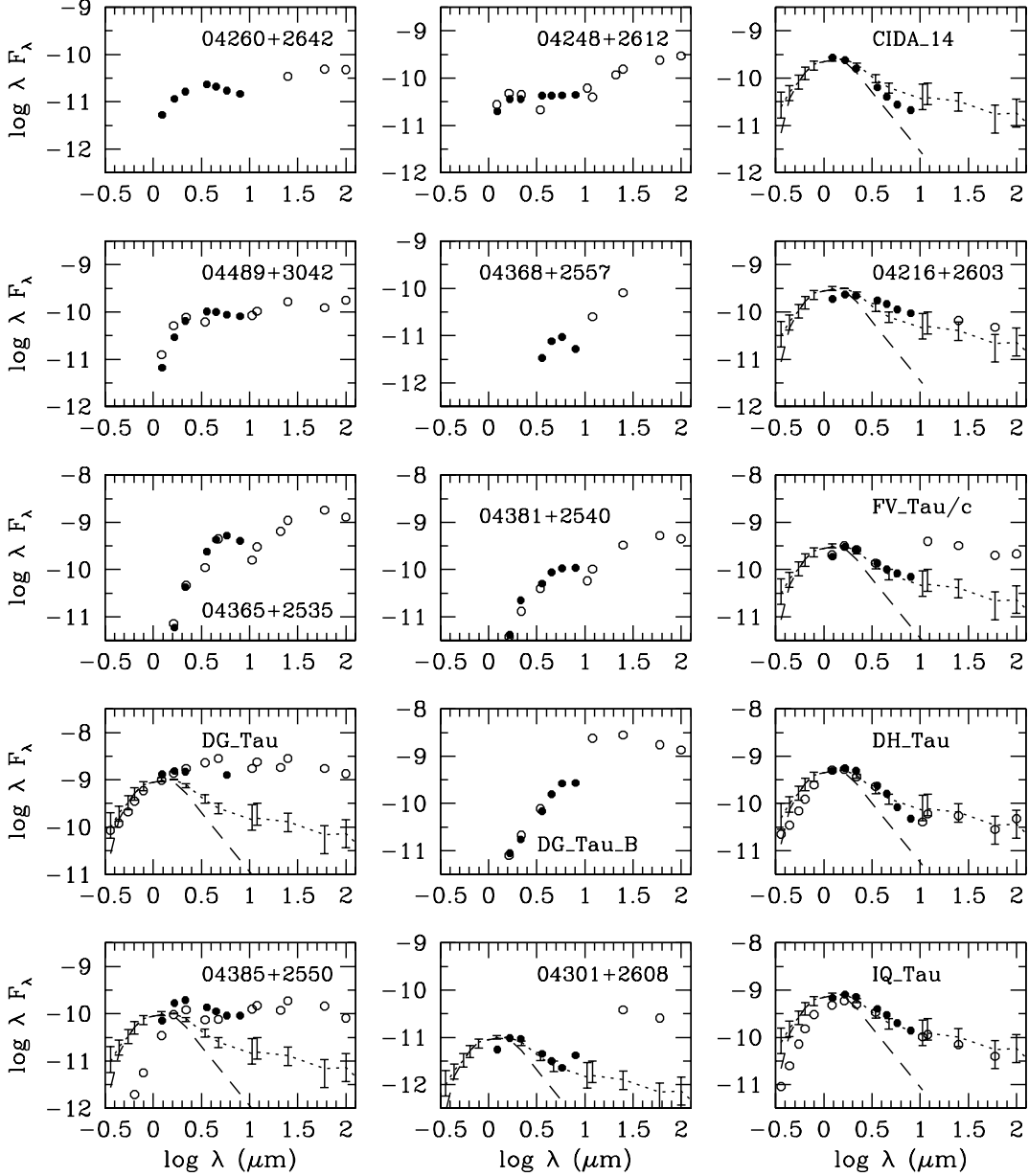


Fig. 5.— SEDs of observed Taurus objects. IRAC fluxes are combined with data from 2MASS (solid circles) and with ground-based and IRAS data taken from Kenyon & Hartmann (1995) (open circles). For some objects we show the (dereddened) SED of the Class III star V819 Tau (dashed line) and the median SED of Taurus Class II K7-M2 objects derived by D’Alessio et al. (1999) (dotted line with error bars denoting the quartiles of the distribution); this median SED illustrates the typical disk emission in Taurus.

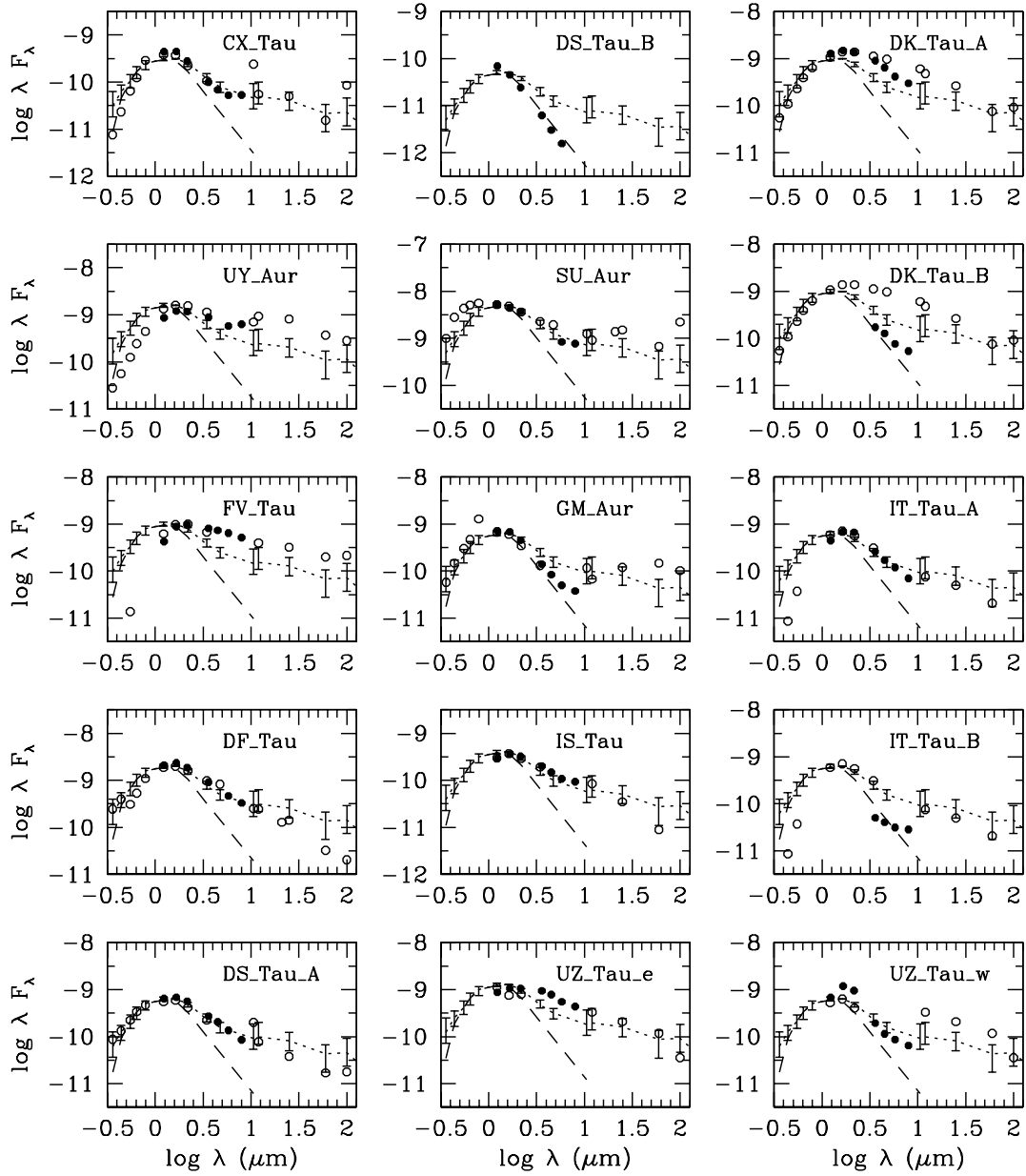


Fig. 6.— Same as Figure 5.

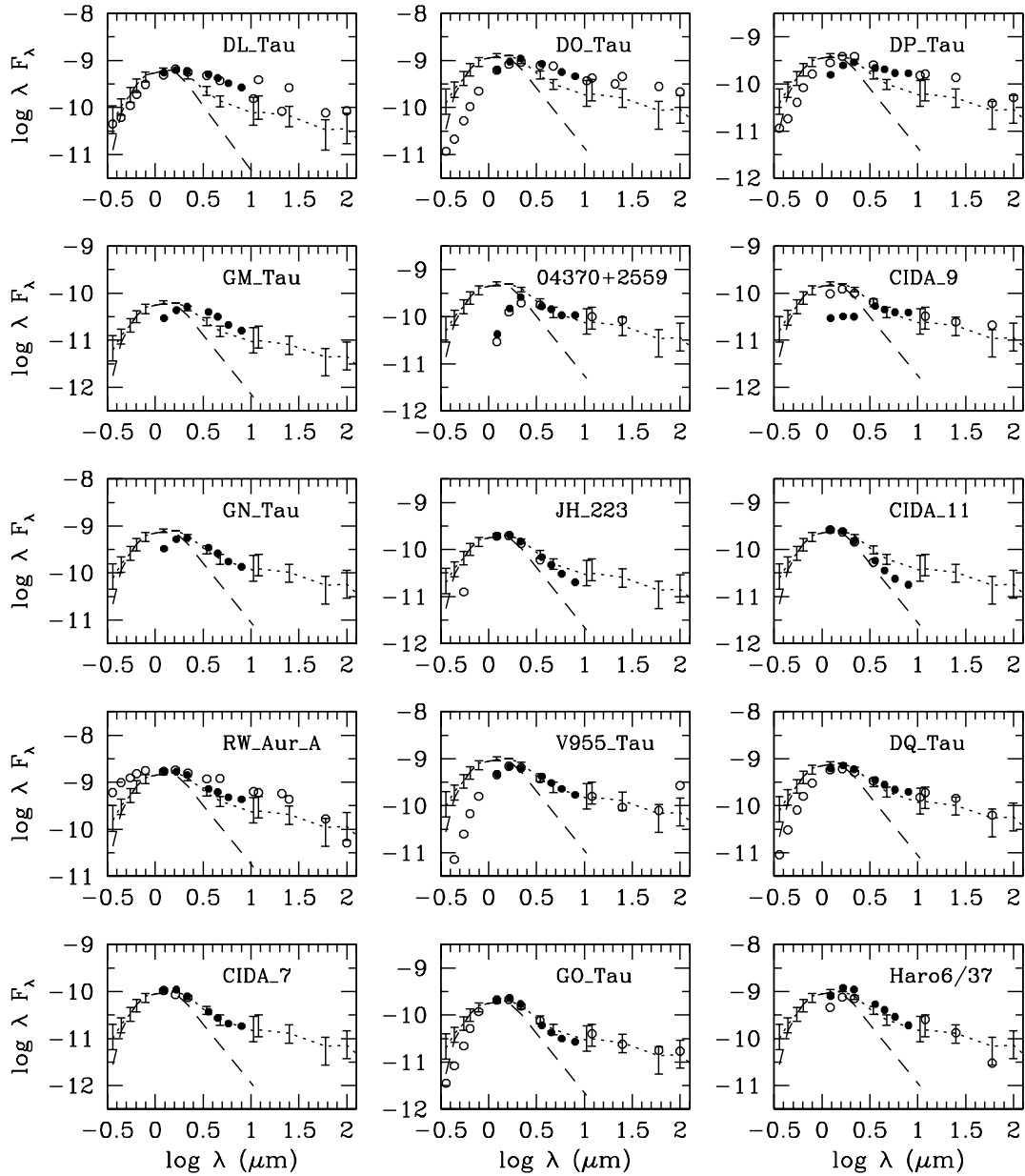


Fig. 7.— Same as Figure 5.

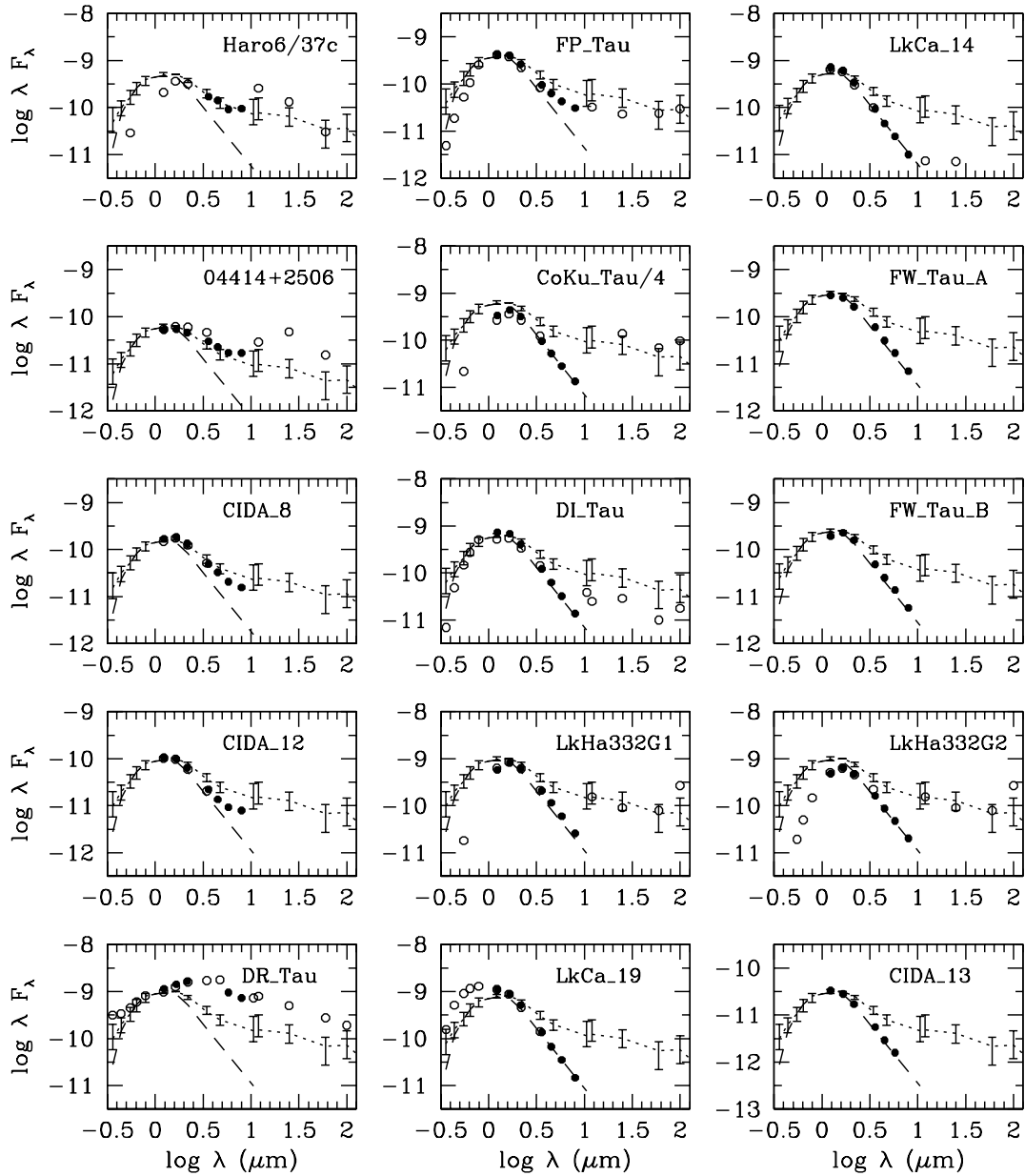


Fig. 8.— Same as Figure 5.



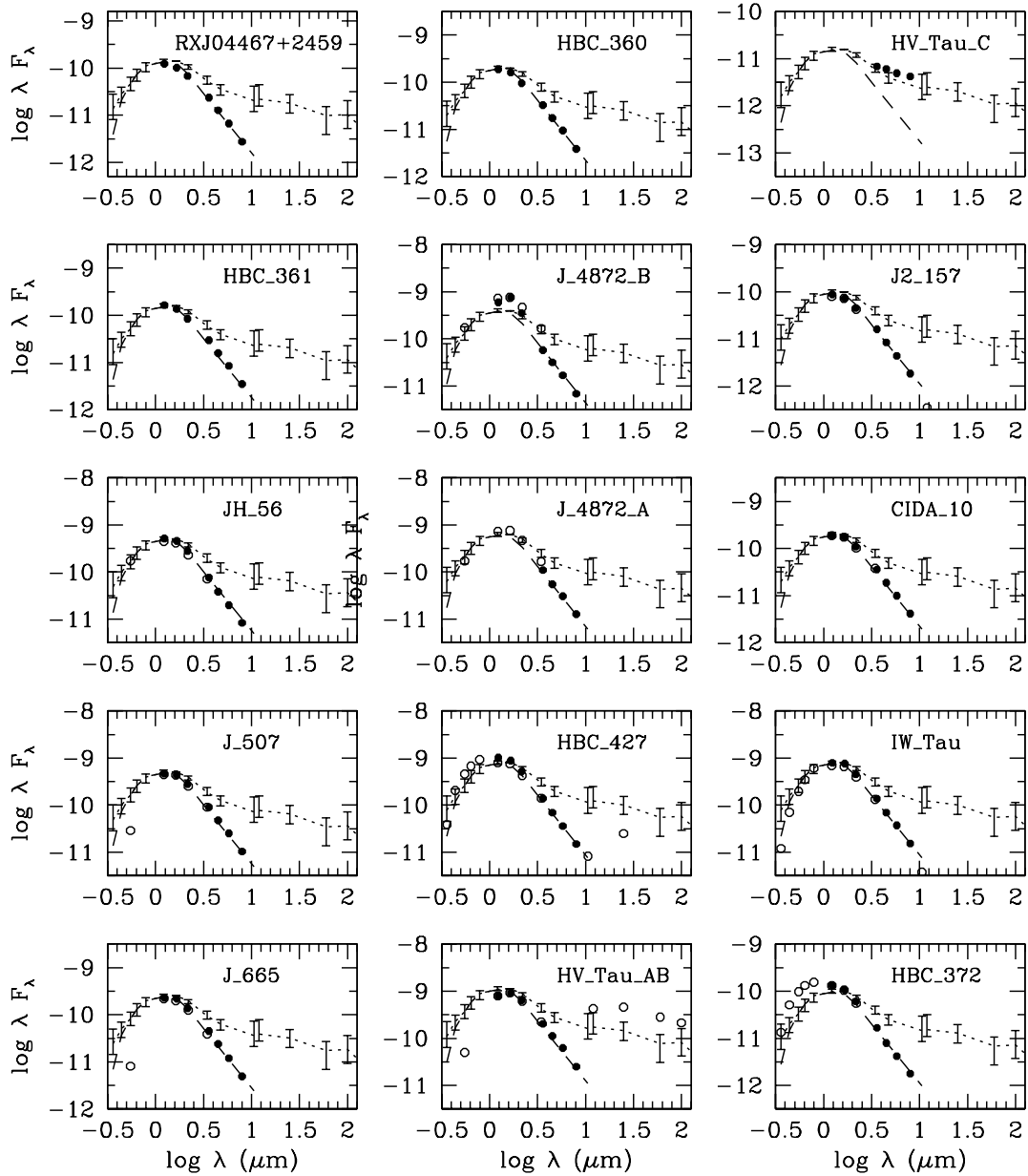


Fig. 9.— Same as Figure 5.

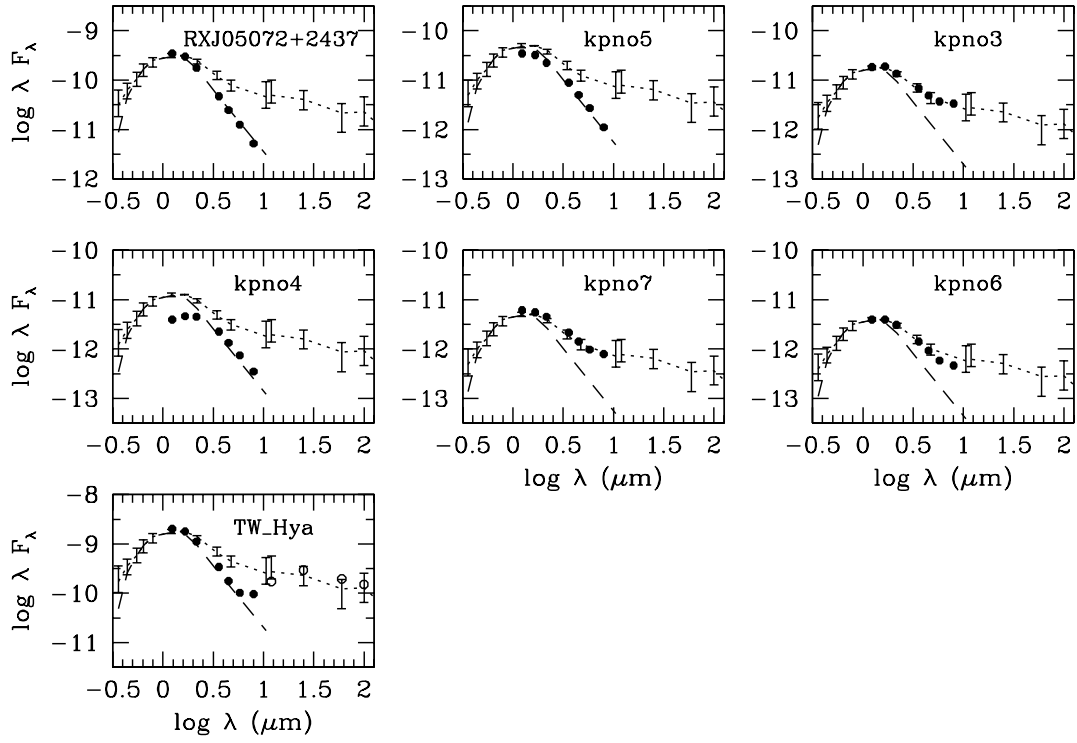


Fig. 10.— Same as Figure 5.

Table 1. IRAC and 2MASS magnitudes

Name	2MASS ID	RA (J2000)	Dec (J2000)	J	H	K <sub>s</sub>	[3.6]	[4.5]	[5.8]	[8]	JD −53000	IRAC type
04260+2642	04290498+2649073	67.27046	26.81819	14.680	13.025	11.883	9.984 ± 0.011	9.388 ± 0.040	8.853 ± 0.008	8.009 ± 0.008	71.676	I
04248+2612	04275730+2619183	66.98861	26.32129	13.235	11.795	11.026	9.335 ± 0.019	8.616 ± 0.014	7.855 ± 0.007	6.812 ± 0.006	71.676	I
04489+3042	04520668+3047175	73.02742	30.78775	14.426	12.021	10.383	8.379 ± 0.011	7.690 ± 0.012	7.095 ± 0.008	6.161 ± 0.012	49.355	I
04368+2557	...	69.97395	26.05224	...	...	...	12.095 ± 0.243	10.484 ± 0.046	9.521 ± 0.088	9.137 ± 0.062	71.637	0
04365+2535	04393519+2541447	69.89638	25.69535	16.905	13.752	10.837	7.466 ± 0.008	6.111 ± 0.008	5.151 ± 0.004	4.420 ± 0.007	71.641	I
04381+2540	04411267+2546354	70.30240	25.77603	17.150	14.137	11.541	9.149 ± 0.033	7.839 ± 0.011	6.882 ± 0.011	5.844 ± 0.003	44.859	I
DG Tau	04270469+2606163	66.76920	26.10399	8.691	7.722	6.992	... ± ...	... ± ...	4.191 ± 0.004	... ± ...	71.684	I/II
DG Tau B	04270266+2605304 <sup>a</sup>	66.76040	26.09137	15.600	13.317	11.819	8.816 ± 0.025	7.209 ± 0.009	5.898 ± 0.012	4.855 ± 0.006	71.684	I/II
04385+2550	04413882+2556267	70.41122	25.94040	11.849	10.123	9.200	8.080 ± 0.014	7.566 ± 0.008	7.048 ± 0.014	6.035 ± 0.002	44.863	II
04301+2608	04331435+2614235	68.30956	26.23946	14.637	13.227	12.496	11.781 ± 0.019	11.451 ± 0.024	11.059 ± 0.037	9.391 ± 0.003	71.672	II
CIDA 14	04432023+2940060	70.83370	29.66794	10.402	9.730	9.408	8.894 ± 0.024	8.681 ± 0.030	8.342 ± 0.003	7.622 ± 0.004	44.895	II
CX Tau	04144786+2648110	63.69909	26.80259	9.867	9.054	8.807	8.406 ± 0.015	8.103 ± 0.037	7.650 ± 0.025	6.623 ± 0.018	45.922	II
04216+2603	04244457+2610141	66.18548	26.17016	10.796	9.753	9.053	7.780 ± 0.011	7.266 ± 0.001	6.821 ± 0.019	6.000 ± 0.013	71.680	II
UY Aur	04514737+3047134	72.94694	30.78664	9.134	7.987	7.239	6.046 ± 0.018	... ± ...	5.042 ± 0.008	3.933 ± 0.003	49.359	II
FV Tau/c	04265440+2606510	66.72671	26.11401	10.800	9.487	8.869	8.079 ± 0.042	7.688 ± 0.031	7.150 ± 0.023	6.319 ± 0.024	71.684	II
FV Tau	04265352+2606543	66.72303	26.11492	9.917	8.325	7.442	6.140 ± 0.043	5.533 ± 0.024	4.932 ± 0.025	4.153 ± 0.024	71.684	II
DH Tau	04294155+2632582	67.42285	26.54902	9.767	8.824	8.178	7.460 ± 0.012	7.184 ± 0.012	7.146 ± 0.028	6.739 ± 0.011	71.684	II
DF Tau	04270280+2542223	66.76133	25.70574	8.171	7.256	6.734	6.006 ± 0.028	... ± ...	5.280 ± 0.008	4.638 ± 0.010	71.691	II
IQ Tau	04295156+2606448	67.46455	26.11205	9.415	8.417	7.779	6.906 ± 0.020	6.503 ± 0.008	6.191 ± 0.025	5.576 ± 0.008	71.691	II
DS Tau A	04474859+2925112	71.95232	29.41969	9.465	8.597	8.036	7.324 ± 0.041	6.909 ± 0.046	6.622 ± 0.027	6.108 ± 0.039	44.898	II
DS Tau B	04474810+2925144	71.95029	29.42064	11.889	11.545	11.453	11.425 ± 0.101	11.495 ± 0.070	11.468 ± 0.070	... ± 0.084	44.898	III <sup>b</sup>
DK Tau A	04304425+2601244	67.68439	26.02352	8.719	7.758	7.096	6.019 ± 0.033	5.672 ± 0.024	5.410 ± 0.039	4.748 ± 0.023	71.695	II
DK Tau B	...	67.68504	26.02320	...	...	...	7.815 ± 0.108	7.429 ± 0.074	7.241 ± 0.111	6.608 ± 0.036	71.695	II
SU Aur	04555938+3034015	73.99697	30.56673	7.199	6.558	5.990	... ± ...	... ± ...	4.638 ± 0.012	3.720 ± 0.007	49.363	II
GM Aur	04551098+3021595	73.79527	30.36610	9.341	8.603	8.283	8.035 ± 0.014	7.878 ± 0.006	7.700 ± 0.009	6.992 ± 0.025	49.363	II
IT Tau A	04335470+2613275	68.47797	26.22423	9.866	8.591	7.860	7.375 ± 0.091	7.111 ± 0.069	6.747 ± 0.029	6.323 ± 0.036	71.656	II
IT Tau B	...	68.47744	26.22378	...	...	...	9.154 ± 0.090	8.669 ± 0.061	8.197 ± 0.064	7.301 ± 0.025	71.656	II
IS Tau	04333678+2609492	68.40302	26.16322	10.323	9.293	8.642	7.654 ± 0.026	7.263 ± 0.024	6.859 ± 0.030	6.015 ± 0.009	71.660	II
UZ Tau e	04324303+2552311	68.17948	25.87520	9.136	8.117	7.354	5.978 ± 0.032	5.461 ± 0.045	5.102 ± 0.029	4.334 ± 0.025	71.664	II
UZ Tau w	04324282+2552314	68.17838	25.87530	9.413	8.006	7.474	7.689 ± 0.045	7.552 ± 0.055	7.107 ± 0.030	6.414 ± 0.024	71.664	II
DL Tau	04333906+2520382	68.41255	25.34346	9.630	8.679	7.960	6.646 ± 0.033	6.124 ± 0.014	5.662 ± 0.010	4.869 ± 0.006	71.664	II
DO Tau	04382858+2610494	69.61883	26.18000	9.470	8.243	7.303	6.084 ± 0.053	... ± ...	5.070 ± 0.011	4.270 ± 0.008	71.641	II
GM Tau	04382134+2609137	69.58858	26.15343	12.804	11.586	10.632	9.400 ± 0.037	8.943 ± 0.025	8.629 ± 0.007	7.918 ± 0.004	71.641	II
04370+2559	04400800+2605253	70.03310	26.09004	12.406	10.248	8.869	7.857 ± 0.010	7.292 ± 0.025	6.868 ± 0.004	5.850 ± 0.004	71.645	II

Table 1—Continued

Name	2MASS ID	RA (J2000)	Dec (J2000)	J	H	K <sub>s</sub>	[3.6]	[4.5]	[5.8]	[8]	JD −53000	IRAC type
GN Tau	04392090+2545021	69.83686	25.75021	10.196	8.893	8.060	7.062 ± 0.011	6.656 ± 0.015	6.344 ± 0.028	5.612 ± 0.004	71.648	II
JH 223	04404950+2551191	70.20581	25.85492	10.750	9.919	9.492	8.810 ± 0.017	8.511 ± 0.025	8.236 ± 0.010	7.677 ± 0.006	44.863	II
RW Aur A	05074953+3024050	76.95599	30.40105	8.378	7.621	7.020	6.268 ± 0.009	5.712 ± 0.011	5.253 ± 0.018	4.345 ± 0.002	47.906	II
V955 Tau	04420777+2523118	70.53225	25.38647	9.811	8.601	7.942	6.849 ± 0.062	6.479 ± 0.032	6.056 ± 0.033	5.350 ± 0.022	44.867	II
V955 Tau B	04420732+2523032	70.53036	25.38409	9.580	8.401	7.945	7.640 ± 0.047	7.543 ± 0.033	7.461 ± 0.024	7.439 ± 0.023	44.867	III <sup>b</sup>
CIDA 7	04422101+2520343	70.58707	25.34251	11.397	10.575	10.169	9.483 ± 0.007	9.105 ± 0.072	8.658 ± 0.010	7.774 ± 0.001	44.871	II
GO Tau	04430309+2520187	70.76235	25.33816	10.712	9.776	9.332	8.960 ± 0.033	8.622 ± 0.032	8.206 ± 0.006	7.357 ± 0.008	44.871	II
DP Tau	04423769+2515374	70.65661	25.25998	10.995	9.689	8.760	7.548 ± 0.020	6.909 ± 0.007	6.369 ± 0.013	5.362 ± 0.003	44.875	II
04414+2506	04442713+2512164	71.11260	25.20420	12.195	11.359	10.761	9.717 ± 0.010	9.305 ± 0.036	8.858 ± 0.009	7.861 ± 0.004	44.879	II
CIDA 9	05052286+2531312	76.34464	25.52488	12.808	11.913	11.161	9.090 ± 0.038	8.555 ± 0.013	7.961 ± 0.006	6.960 ± 0.004	49.375	II
CIDA 8	05044139+2509544	76.17193	25.16473	10.913	10.011	9.597	9.189 ± 0.024	8.913 ± 0.028	8.665 ± 0.029	7.956 ± 0.006	49.375	II
CIDA 11	05062332+2432199	76.59673	24.53845	10.421	9.712	9.459	9.002 ± 0.017	8.808 ± 0.014	8.497 ± 0.009	7.810 ± 0.008	49.379	II
CIDA 12	05075496+2500156	76.97855	25.00397	11.415	10.705	10.400	10.039 ± 0.029	9.858 ± 0.006	9.525 ± 0.013	8.688 ± 0.017	49.383	II
DQ Tau	04465305+1700001	71.72082	16.99956	9.511	8.544	7.981	7.037 ± 0.002	6.569 ± 0.011	6.097 ± 0.008	5.199 ± 0.004	70.852	II
DR Tau	04470620+1658428	71.77560	16.97816	8.845	7.799	6.874	... ± ...	... ± ...	4.499 ± 0.008	3.786 ± 0.013	70.852	II
Haro6/37	04465897+1702381	71.74578	17.04369	9.239	7.991	7.310	6.581 ± 0.073	6.170 ± 0.038	5.802 ± 0.022	5.228 ± 0.023	70.852	II
Haro6/37c	...	71.74628	17.04428	...	...	...	7.838 ± 0.078	7.320 ± 0.073	7.041 ± 0.033	5.988 ± 0.024	70.852	II
FP Tau	04144730+2646264	63.69677	26.77361	9.897	9.175	8.873	8.455 ± 0.011	8.194 ± 0.017	7.880 ± 0.008	7.218 ± 0.031	45.922	II
LkCa 14	04361909+2542589	69.07929	25.71599	9.336	8.713	8.580	8.474 ± 0.034	8.540 ± 0.018	8.485 ± 0.005	8.441 ± 0.005	71.652	III
CoKu Tau/4	04411681+2840000	70.31945	28.66627	10.163	9.077	8.656	8.446 ± 0.010	8.394 ± 0.020	8.321 ± 0.007	8.116 ± 0.003	44.895	III
FW Tau A	04292971+2616532	67.37374	26.28136	10.340	9.675	9.388	8.957 ± 0.053	8.964 ± 0.045	8.881 ± 0.026	8.819 ± 0.024	71.688	III <sup>b</sup>
FW Tau B	04292887+2616483	67.37028	26.28007	10.784	9.792	9.417	9.204 ± 0.049	9.200 ± 0.042	9.104 ± 0.030	9.030 ± 0.023	71.688	III <sup>b</sup>
DI Tau	04294247+2632493	67.42670	26.54652	9.323	8.599	8.391	8.186 ± 0.033	8.195 ± 0.026	8.179 ± 0.014	8.091 ± 0.008	71.684	III
LkH332G1	04420732+2523032	70.53003	25.38376	9.580	8.401	7.945	7.602 ± 0.024	7.534 ± 0.020	7.509 ± 0.052	7.399 ± 0.027	44.867	III
LkH332/G2	04420548+2522562	70.52239	25.38183	9.787	8.663	8.227	7.877 ± 0.015	7.834 ± 0.022	7.751 ± 0.007	7.660 ± 0.005	44.867	III
LkCa 19	04553695+3017553	73.90353	30.29824	8.870	8.318	8.148	8.078 ± 0.017	8.128 ± 0.020	8.087 ± 0.010	8.025 ± 0.005	49.367	III
CIDA 13	04391586+3032074	69.81579	30.53504	12.680	12.069	11.834	11.554 ± 0.026	11.538 ± 0.007	11.455 ± 0.058	... ± ...	73.113	III
RXJ04467+2459	04464260+2459034	71.67705	24.98389	11.261	10.667	10.338	9.980 ± 0.006	9.929 ± 0.001	9.896 ± 0.012	9.837 ± 0.012	44.883	III
HBC 360	04043936+2158186	61.16364	21.97144	10.798	10.171	9.966	9.624 ± 0.052	9.589 ± 0.019	9.517 ± 0.029	9.473 ± 0.022	46.426	III
HBC 361	04043984+2158215	61.16562	21.97226	10.939	10.353	10.101	9.728 ± 0.009	9.704 ± 0.015	9.624 ± 0.026	9.572 ± 0.020	46.426	III
J 4872 B	04251767+2617504	66.32294	26.29675	9.537	8.475	8.545	9.007 ± 0.062	8.942 ± 0.027	8.877 ± 0.030	8.848 ± 0.022	71.699	III
J 4872 A	...	66.32377	26.29731	...	...	...	8.307 ± 0.042	8.337 ± 0.044	8.230 ± 0.022	8.164 ± 0.023	71.699	III
JH 56	04311444+2710179	67.80986	27.17122	9.705	9.036	8.794	8.703 ± 0.027	8.742 ± 0.017	8.707 ± 0.010	8.631 ± 0.007	71.715	III
J 507	04292071+2633406	67.33598	26.56081	9.821	9.089	8.791	8.521 ± 0.014	8.497 ± 0.028	8.446 ± 0.005	8.398 ± 0.007	71.699	III

Table 1—Continued

Name	2MASS ID	RA (J2000)	Dec (J2000)	J	H	K <sub>s</sub>	[3.6]	[4.5]	[5.8]	[8]	JD −53000	IRAC type
HBC 427	04560201+3021037	74.00796	30.35061	8.958	8.317	8.129	8.056 ± 0.018	8.095 ± 0.025	8.055 ± 0.013	8.001 ± 0.004	49.371	III
J 665	04315844+2543299	67.99329	25.72457	10.585	9.828	9.559	9.283 ± 0.019	9.243 ± 0.070	9.257 ± 0.015	9.200 ± 0.006	71.668	III
HV Tau AB	04383528+2610386	69.64704	26.17735	9.227	8.284	7.906	7.644 ± 0.094	7.578 ± 0.036	7.468 ± 0.022	7.441 ± 0.025	71.641	III
HV Tau C	...	69.64792	26.17816	...	...	...	11.327 ± 0.139	10.743 ± 0.045	10.223 ± 0.045	9.379 ± 0.040	71.641	II <sup>b</sup>
IW Tau	04410470+2451062	70.26911	24.85132	9.244	8.479	8.275	8.067 ± 0.018	8.092 ± 0.012	8.022 ± 0.002	7.972 ± 0.003	44.879	III
J2 157	04205273+1746415	65.21945	17.77789	11.618	11.040	10.776	10.401 ± 0.017	10.383 ± 0.017	10.356 ± 0.008	10.278 ± 0.003	72.336	III
HBC 372	04182147+1658470	64.58923	16.97939	11.175	10.603	10.464	10.355 ± 0.003	10.443 ± 0.015	10.405 ± 0.036	10.313 ± 0.022	72.340	III
CIDA 10	05061674+2446102	76.56924	24.76910	10.792	10.091	9.815	9.522 ± 0.018	9.508 ± 0.028	9.457 ± 0.018	9.393 ± 0.027	49.383	III
RXJ05072+2437	05071206+2437163	76.79977	24.62079	10.141	9.490	9.297	9.220 ± 0.023	9.209 ± 0.050	9.208 ± 0.006	9.144 ± 0.006	49.387	III
KPNO5	04294568+2630468	67.43999	26.51254	12.640	11.918	11.536	11.036 ± 0.015	10.951 ± 0.006	10.868 ± 0.031	10.826 ± 0.028	71.684	III <sup>b</sup>
KPNO3	04262939+2624137	66.62216	26.40343	13.323	12.501	12.079	11.319 ± 0.031	10.978 ± 0.014	10.535 ± 0.010	9.618 ± 0.003	71.703	II <sup>b</sup>
KPNO4	04272799+2612052	66.86636	26.20104	14.997	14.025	13.281	12.531 ± 0.015	12.381 ± 0.024	12.270 ± 0.160	12.069 ± 0.319	71.703	III <sup>b</sup>
KPNO7	04305718+2556394	67.73805	25.94391	14.521	13.828	13.272	12.577 ± 0.017	12.311 ± 0.039	11.979 ± 0.071	11.194 ± 0.062	71.695	II <sup>b</sup>
KPNO6	04300724+2608207	67.52984	26.13874	14.995	14.197	13.689	13.033 ± 0.033	12.781 ± 0.036	12.535 ± 0.168	11.770 ± 0.114	71.711	II <sup>b</sup>
TW Hya	11015191-3442170	165.46632	-34.70472	8.217	7.558	7.297	7.13 ± 0.03	7.07 ± 0.01	6.93 ± 0.02	5.98 ± 0.01	... <sup>c</sup>	II

<sup>a</sup>Used 2MASS extended source magnitudes for DG Tau B

<sup>b</sup>New classification, based on IRAC data in this paper; <sup>c</sup>Observation date JD = 52993.131

Note. — The position of CIDA 12 in Briceño et al. (1993) is in error; should be (J2000) 5h 07m 54.98s +25d 00m 15s.